The effect of fibre orientation on fatigue crack propagation in CFRP

Finite fracture mechanics modelling for open-hole configuration

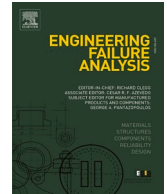Monticeli, Francisco Maciel; Fuga, Felipe Ruivo; Arbelo, Mariano Andrés; Donadon, Maurício Vicente

Important note
To cite this publication, please use the final published version (if applicable).
Please check the document version above.

The effect of fibre orientation on fatigue crack propagation in CFRP: Finite fracture mechanics modelling for open-hole configuration

Francisco Maciel Monticeli [a],[*], Felipe Ruivo Fuga [b], Mariano Andrés Arbelo [b], Maurício Vicente Donadon [b]

[a] Department of Aerospace Structures and Materials, Faculty of Aerospace Engineering, Delft University of Technology, Delft, the Netherlands
[b] Aeronautical Engineering Division, Technological Institute of Aeronautics (ITA), São José dos Campos, Brazil

ARTICLE INFO

ABSTRACT

The demand to capture translaminar crack growth under fatigue loading scenarios led this work contribution to carry out the Finite Fracture Mechanics (FFM) method in fatigue damage growth and the application of the Paris model to generate the translaminar damage propagation prediction. The purpose of this study is to analyse the effect of fibre orientation on translaminar crack propagation rate using the FFM model, which includes cycle damage increment estimation and fractographic analysis. The results confirm the feasibility of FFM in predicting crack growth and estimating life under cyclic loading. However, C-scan analysis and the revised crack propagation direction are critical in determining the realistic crack length, considering adhesive failure along the fibre direction. Additionally, this work contribution is also related to the application of the Paris model (based on dL/dN vs ΔK) to generate the translaminar damage propagation prediction model. The most dominant damage mechanism was the splitting pattern, which changed the aspect of failure for each laminate architecture as a function of fibre orientation. The laminate with multidirectional fibre orientation exhibited higher resistance to translaminar crack propagation due to the growth of splitting and delamination in multiple directions. The fibre orientation changed the propagation path, which influenced the fracture toughness and crack propagation rate behaviour.

1. Introduction

The use of laminated composites as a lightweight material in industrial sectors has increased due to the need to preserve natural resources and reduce CO_2 emissions [1]. However, this has resulted in a demand for more complex design methods. This demand is often significant limitation for carbon fibre composite applications, mainly for structural components [2,3]. An example is bolted joint for attaching multiple parts, where holes in the laminate can act as a raiser, potentially leading to catastrophic failure in this region [4,5]. These limitations can arise from hole fabrication/drilling [6], exposure to environmental conditions [7], or the mechanical behaviour resulting from the discontinuity in the fibre created by the hole [8].

Analysing the initiation and propagation of intralaminar damage is a complex challenge in fracture mechanics. Conventional

---

methods, such as the stress intensity factor or area methods, may lead to unrealistic results for estimating fracture toughness, as they depend on the specimen geometry to account for the deformations during the crack opening stage [9]. This problem can be even more evident during crack propagation, as the damage progression generates more significant deformations that override the real R- and J-curves [10]. Recent studies have shown that applying tensile loads to notched laminates (i.e., single-edge notch) can reduce errors caused by other deformation modes for compact tension configuration, such as delamination, compression, and shear [11].

Failure patterns in open-hole configuration laminates typically initiate with matrix cracking, followed by splitting, delamination, and fibre rupture [12]. Determining the sequence of failure mechanisms is essential to developing an accurate predictive model. The Tsai-Wu criterion has been found to provide an appropriate relationship with experimental data by incorporating the primary failure mechanisms, such as tensile and compressive fibre failure and matrix failure [13]. Following the linear fracture mechanics field, Griffith introduced the energy-based model [14], in which a crack propagates when the energy is greater than or equal to the surface energy. Subsequently, Irwin [15] established the stress intensity factor (SIF), which has been considered a critical parameter in fracture mechanics for quantifying the stress field at the crack tip. Paris [16] further developed the failure envelope to describe the relationship between crack propagation rate and energy dissipation. However, open-hole laminates restrict the application of those models, thereby limiting their usefulness in assessing damage growth tolerance.

To overcome the aforementioned limitation, Chang et al. [17] formulated an analytical progressive damage analysis methodology to investigate the tensile failure behaviour of laminated composites with open-hole feature. Their findings revealed a significant influence of the ply orientation on the damage mechanism and strength of the material. Also, Whitney and Nuismer [18] presented a novel approach for analysing composite laminates, combining normal stresses and unnotched tensile strength criteria to predict the residual stress distribution and notch effects. This methodology enables accurate predictions of size effects without relying on linear elastic fracture mechanics.

The fracture behaviour of laminate open-hole is challenging to study due to the abrupt failure, which hinders damage monitoring and control. To address this issue, Leguillon [19] introduced energy and stress criteria that allowed the Griffith criterion to a measured crack size. Following the same criteria, Cornetti et al. [20] proposed a failure criterion within the framework of finite fracture mechanics (FFM) framework under quasi-static loading. This model used the critical stress intensity factor and the nominal stress of the uncracked sample to track fracture propagation and generate a prediction model based on the material properties and geometry. Similarly, Camanho et al. [20] proposed a method based on a continuum damage model to predict strength and size effects in notched carbon-epoxy laminates. They identified the size effect caused by hole diameter and the development of a fracture process zone prior to final failure, conducting the linear elastic fracture mechanics (LEFM) as a feasible approach to address such a problem. The extension of the FFM for laminates with a central hole was evaluated, where a damage zone exhibits a linear relationship with traction exerted and crack opening [21]. The FFM approach has been validated for open-hole tensile [21] and open-hole compression [22] under quasi-static loading. These studies provide valuable insights into fracture behaviour for open-hole specimens, enabling improved monitoring and control of crack growth associated with stress intensity factor. Following Tserpes et al. [23], The FFM provides a feasible comparative and preliminary analysis, based on reasonable assumptions about interface properties, to determine optimal solutions in terms of geometry, components and loading conditions. However, the main challenge lies in the potential extension of the method to include fatigue loading scenarios. To this end, this work contribution is related to the use of FMM in fatigue damage growth and the application of the Paris model to generate the damage propagation rate (*dL/dN*) curve in relation to the strain energy release ratio, and thus to generate a translaminar damage propagation prediction model under cyclic loading.

Considering the possibility of modelling lifetime estimation based on finite fracture mechanics (FFM), some questions remain, such as how fibre orientation affect the modelling of translaminar fracture? Using the crack size prediction generated by the FFM model, would it be possible to design the translaminar crack propagation rate? In order to extend the application of the model to include fatigue loading and feasibility for different architectures, these issues are important. To answer the above questions, this work aims to predict the intralaminar crack propagation for open-hole composites under cyclic loading considering fibre orientation effect using FFM modelling. For that purpose, this work comprises: *i)* the generation of the SN-curve, *ii)* inherent characteristic length growth (i.e., crack propagation) through cycles, *iii)* the effect of fibre orientation on stiffness decay and crack growth, *iv)* the application of the fatigue failure criterion based on FFM to estimate the cycle damage increment related to the crack propagation rate, and *vi)* the fractographic analysis of each composite architecture.

2. Finite fracture mechanics model for open-hole tensile

The FFM model operates on energetic principles, whereby the energy required to propagate the crack size *L* (characteristic length) is directly related to the material fracture toughness. The model assumes that the stress at the crack tip, spanning distance *L*, is analogous to the stress of the unnotched composite, as given by Eq. (1) [21,24]. Furthermore, the relation of crack size *L* and the stress intensity factor is established in the Eq. (2) [24]. By solving the system comprising Eqs. (1) and (2), the size of *L* can be determined for a given set of critical SIF (K_{IC}) and unnotched stress (X_T) parameters. This approach provides a persuasive and scientific method for analysing the fracture behaviour.

$$\frac{1}{L}\int_R^{R+L} \sigma_{yy}(x,0)dx = X_T \qquad (1)$$

$$\frac{1}{L}\int_R^{R+L} K_I^2(a)da = K_{IC}^2 \qquad (2)$$

where, L is the crack length, R is the hole radius, $\sigma_{yy}(x,0)$ is the tensile stress distribution along the x-axis, X_T is the unnotched laminate strength, K_{IC} is the mode I fracture toughness of the laminate.

In particular, the lay-up of a laminate can induces brittle or pull-out failure modes, and the ultimate failure due to macro-crack propagation is observed to occur along the transverse direction of the applied load, as supported by previous studies [24,25]. Fig. 1 shows the continuous crack size generated by the damaged region at failure, as predicted by the aforementioned model. In addition, the stress criterion predicts failure when the average stress over a distance L from the notch exceeds or reaches the strength of the unnotched laminate. The effective crack length L is dependent on the hole diameter and the remotely applied stress σ_r required to create a damage zone that develop the crack length from the hole edge (radius R) [21]. These findings provide a scientific framework for analysing the failure behaviour of open-hole laminates.

Eq. (3) describes the distribution of tensile stress in front of the hole edge over the distance L in the translaminar direction of propagation.

$$\sigma_{yy}(x,0) = \frac{\sigma_r}{2F_0}\left\{2 + \left(\frac{R}{x}\right)^2 + 3\left(\frac{R}{x}\right)^4 - (K_T^\infty - 3)\left[5\left(\frac{R}{x}\right)^6 - 7\left(\frac{R}{x}\right)^8\right]\right\}$$

(3)

The stress analysis of an infinite plate containing an open-hole involves the determination of remote stress (σ_r), stress concentration factor (K_T^∞), and the finite width correction factor ratio ($1/F_0$) using Eqs. (4)–(6), according to reference [22]. For the following equation, the in-plane stiffness matrix components of the laminate, denoted by A_{ij}, are derived by applying the classical lamination theory defined in the Appendix A, and w is the specimen width.
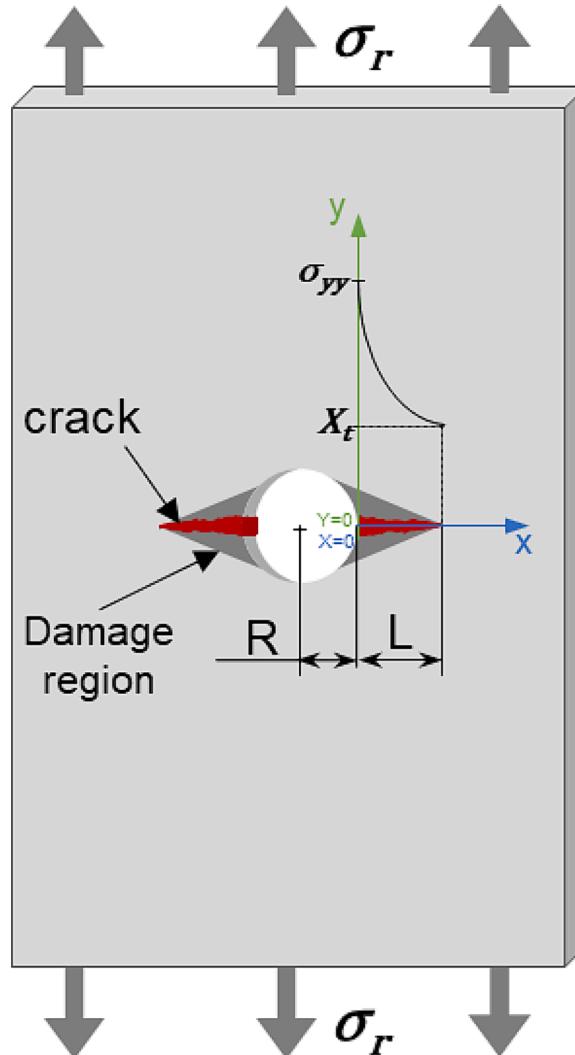

Fig. 1. Translaminar cracks failure mode under an opening mode loading.

$$K_T^\infty = 1 + \sqrt{\frac{2}{A_{22}}\left(\sqrt{A_{11}A_{22}} - A_{12} + \frac{A_{11}A_{22} - A_{12}^2}{2A_{66}}\right)} \tag{4}$$

$$\frac{1}{F_0} = \frac{3(1 - 2R/w)}{2 + (1 - 2R/w)^3} + \frac{(K_T^\infty - 3)}{2}\left[1 - \left(\frac{2R}{w}M\right)^2\right]\left(\frac{2R}{w}M\right)^6 \tag{5}$$

$$M^2 = \frac{\sqrt{1 - 8\left[\frac{3(1-2R/w)}{2+(1-2R/w)^3} - 1\right]} - 1}{2(2R/w)^2} \tag{6}$$

The symmetry of the two sides of propagation leads to the definition of the stress intensity factor for a laminate with a central hole, as shown in Eq. (7). Furthermore, the correction factors F_1 and F_2 are explained by Eqs. (8) and (9) respectively [21].

$$K_I = \sigma_r F_1 F_2 \sqrt{\pi a} \tag{7}$$

$$F_1 = \sqrt{1 - \frac{R}{a}}\left[1 + 0.358\left(\frac{R}{a}\right) + 1.425\left(\frac{R}{a}\right)^2 - 1.578\left(\frac{R}{a}\right)^3 + 2.156\left(\frac{R}{a}\right)^4\right] \tag{8}$$

$$F_2 = \sqrt{\sec\left(\frac{\pi D}{2w}\right)\sec\left(\frac{\pi a}{w}\right)} \tag{9}$$

where, a represents the hole radius plus crack length $(R + L)$.

The numerical integration method employing Simpson's rule was used to determine the numerical value of crack length (L) and solve Eqs. (1) and (2). The stress around the open-hole is evaluated, and the inherent crack length for static loading is determined. However, microcracks generated during the cyclic loading can alter the length of the damaged region and consequently affect the size of L. A cyclic relationship between crack size per cycle and the corresponding energy of the material is established by subjecting it to a subsequent series of cyclic loads at constant load amplitude and applying a new static loading until failure, as shown in Eqs. (10) and (11) [26], where N is the number of cycles. The ratio of effective crack length per cycle provides the growth rate of the effective crack length in the damaged region (dL/dN) as a function of fracture toughness. This relationship enables the creation of a predictive model for lifetime damage control. This model will also be used to compare the effect of fibre architecture variation. Fig. 2 illustrates the flowchart of each step and the data obtained at each stage.

$$\frac{1}{L}\int_R^{R+L}\sigma_{yy}(x, 0)dx = X_t(N); for X_t(N) = \frac{1}{L}\int_R^{R+L}\sigma_{yy}(x, 0)dx = C_1 N^{m_1} \tag{10}$$

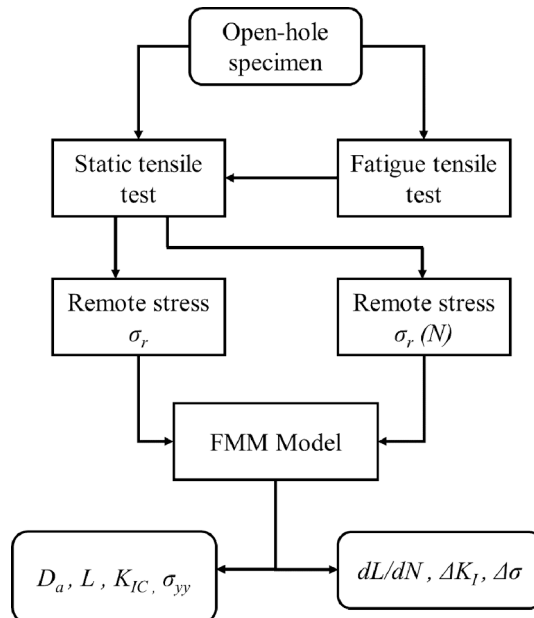**Fig. 2.** Methodology flowchart.

$$\frac{1}{L}\int_R^{R+L}K_I^2(a)da = K_{IC}^2(N); for K_{IC}^2(N) = \frac{1}{L}\int_R^{R+L}K_I^2(a)da = C_2 N^{n_2} \tag{11}$$

where, N is the cycle number, C_i and n_i are fitting parameters.

3. Material characterisation

The current study utilised plain weave carbon fabric Hexcel®HexForce™AGP193-P as reinforcement while the matrix consisted of the epoxy resin Huntsman Araldite® LY5052 and a polyamines mixture hardener, Huntsman Aradur® 5052. The laminates were manufactured using the resin transfer moulding (RTM) process. The laminate was cured at a temperature of 24 °C for 120 min at 5 bar, cured at 100 °C for 4 h and subsequently at 24 °C for 24 h, following supplier recommendations [27]. Two lay-ups were selected: cross-ply $[0/90]_{4S}$ and quasi-isotropic $[\pm45/0/90]_{2S}$, corresponding to laminates with a nominal thickness of 2 mm and 50 % of reinforcement. As the FFM model was originally developed for UD laminate, the purpose of this paper is to verify the possibility of using cross-ply and quasi-isotropic configurations and their respective interaction with translaminar fracture. In addition, both lay-ups are commonly used and provide a significant contribution to the industrial sector [28]. The size of each specimen was $200 \times 50 \times 2$ mm^3, with a 10 mm diameter hole at the middle of the specimen, following the ratio of width/diameter $(w/2R) = 5.0$.

The ply elastic properties, including longitudinal and transverse Young's modulus ($E_1 = E_2 = 51.83$ GPa), ply shear modulus ($G_{12} = 2.82$ GPa), and major Poisson's ratio ($v_{12} = 0.064$) [11], were measured in a previous investigation following ASTM D3039 and ASTM D3518 standards. Additionally, the unnotched tensile strength of the laminate was measured using five test specimens following ASTM standard D-3039. Table 1 presents the effective elastic properties of each laminate, followed by respective unnotched stress.

Testing procedures were conducted using an MTS servo-hydraulic machine with a 250 kN load cell. The first group were the static displacement-controlled tests for laminates with holes and unnotched in three replicates for each. The static tests were conducted at a rate of 2 mm/min until de complete fracture of the specimen.

The fatigue tests were carried out on the same machine. The test was performed under load control, with the maximum stress being 85 % of the ultimate stress in the static test. The relationship between the minimum and maximum stresses follows the ratio of 0.1 ($\sigma_{min}/\sigma_{max} = 0.1$). The frequency used was 7 Hz. A constant amplitude was maintained throughout the fatigue tests.

4. Results and discussions

4.1. Damage region interpretation

In this section, the damage between the plies is incorporated into the proposed model for the damaged region for each material. The ultrasonic C-scan scheme for specimens under cyclic loading (Fig. 3), where the cross-ply sequence is shown in Fig. 3a and $[\pm45/0/90]$ is shown in Fig. 3b. An ultrasonic C-scan image was captured for the pristine/unload specimen before testing, and subsequent images were taken after cyclic loading. As the number of the cycles increases, the damage area varies between both laminate configurations.

The cross-ply composite exhibits low damage in the transverse direction and shows damage propagation in the same direction of the applied load, i.e., parallel to the vertical fibres. On the other hand, the laminate $[\pm45/0/90]$ exhibits the direction of 45° internal damage propagation. The main failure pattern observed is the splitting [29]. This phenomenon occurs in fibre-reinforced polymers when a transverse or shear load is applied, leading to fibre displacement relative to the matrix and creating an interlaminar defect [29,30]. The splitting effect is similar to a wedge, where the composite layers separate, forming a crack that can propagate through the structure [31]. This process is initiated when the shear stress exceeds the interlaminar strength of the composite, reducing the stress sufficiently to cause fibre fracture (translaminar propagation) [27].

Li et al. [6] observed that the splitting effect occurs along the fibre orientation, indicating that laminates with a 45° orientation are less prone to transverse fibre fracture. The failure area mainly involves delamination or splitting in an X-pattern shape. Moreover, the multidirectional fibres in the laminate $[\pm45/0/90]$ increase the probability of splitting in different directions, following the fibre orientation and affect the residual stress degradation significantly different from the cross-ply lay-up. The results presented in Fig. 3a support the contribution of the fibre orientation to the damage propagation along the laminate.

The measurements of crack propagation considering the addition of the C-scan damaged region during fatigue loading are conducted in this section. The damaged region was measured as an equivalent damage length (D_a) in regions with wave attenuation by C-scan. The equivalent damage length was measured between the initial hole diameter and the edge of the attenuated region. The D_a measurements steps were added in the Appendix B.

Table 1
Composite effective elastic properties.

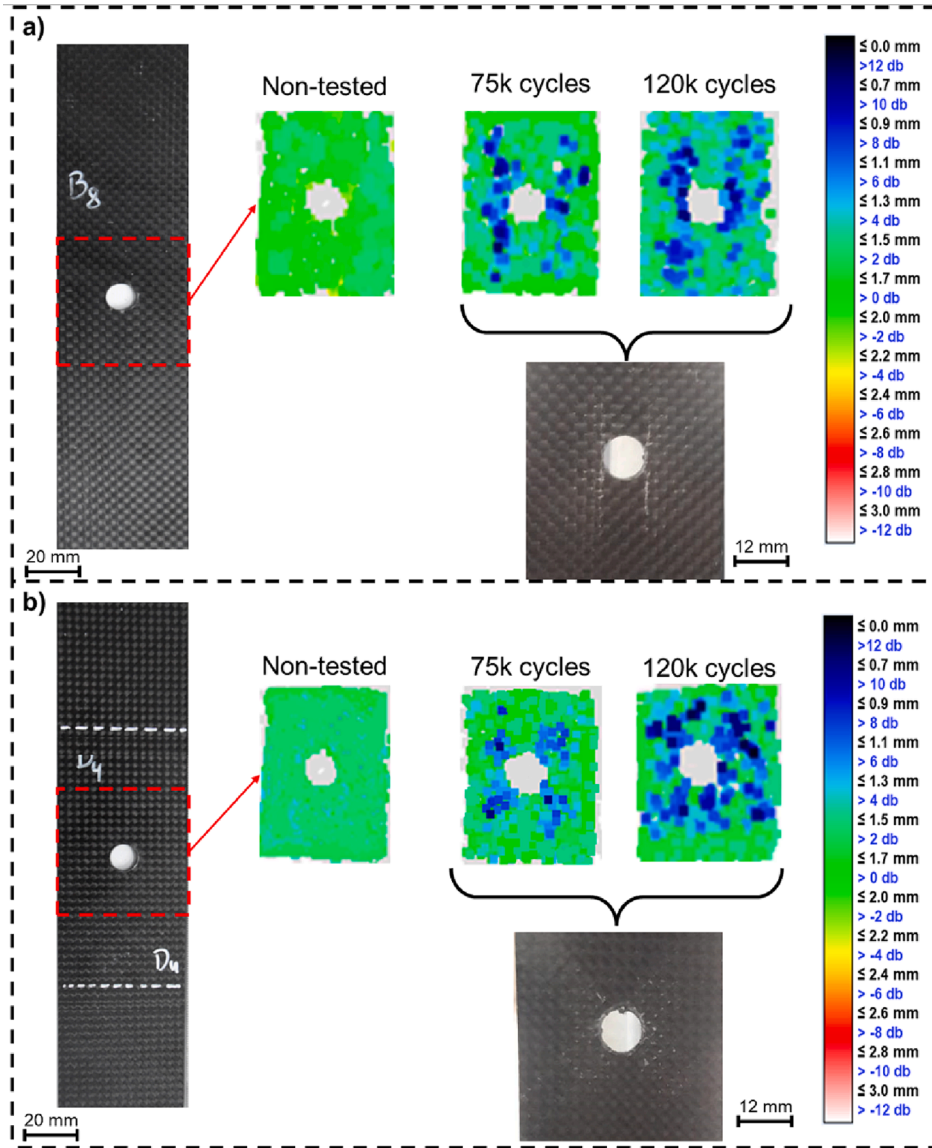| Laminate	E_x	E_y	G_{xy}	v_{xy}
	(GPa)	(GPa)	(GPa)	
[0/90]	51.83	51.83	2.82	0.064
[±45/0/90]	36.46	36.46	13.59	0.342

Fig. 3. C-scan considering cyclic loading: a) [0/90] and b) [±45/0/90].

4.2. Mechanical test results

The findings of the mechanical tests conducted on both laminate architectures are shown in Table 2. The unnotched stress results under static loading for the [0/90] laminate is 764.90 ± 15.73 MPa, and for the [±45/0/90] is 513.65 ± 31.78 MPa. Meanwhile, the ultimate stress for open-hole laminates is 488.50 ± 12.88 MPa and 408.12 ± 5.51 MPa for [0/90] and [±45/0/90] laminates, respectively. The [0/90] laminate shows a 36 % reduction in strength while the [±45/0/90] laminate shows a 20 % reduction due to hole insertion. This suggests that the cross-ply laminate is more sensitive to the notch. The low coefficient of variation presented (≈ 3.74 %) indicates that the specimen exhibited homogeneous behaviour. Therefore, the average values were used to model finite fracture mechanics.

The equivalent damage length (D_a), crack length (L), residual remote stress under static loading (σ_r) and SIF (K_{IC}) are presented in Table 2. The following trend is observed: as the number of cycles increases, the length of the region affected by microfractures (L) also increases. The observed trend supports the inverse relationship described in Eq. (1), which states that the tensile strength (σ_r) decreases as the length of the affected region (L) increases. This result can be attributed to the damage caused during load cycling, which increases the crack length and affects the formation of the damaged region. There is also a direct correlation between the inherent crack length (L) and the stress intensity factor. As the crack length increases, there is a proportional increase in the stress intensity factor (K) [32,33]. This finding is consistent with Eq. (7), which describes a proportional relationship between K and the crack length (L) of the

Table 2
Experimental results for both lay-ups.

[0/90]					
D_a	L	σ_r	Cycles N	K_{IC}	X_T
(mm)	(mm)	(MPa)	($\times 10^3$)	(MPa $\bullet \sqrt{m}$)	(MPa)
5.00	3.64	488.50	0	71.34	764.90
6.03	3.89	480.86	75	80.05	
7.01	4.11	471.72	120	88.71	

[±45/0/90]					
D_a	L	σ_r	Cycles N	K_{IC}	X_T
(mm)	(mm)	(MPa)	($\times 10^3$)	(MPa$\bullet \sqrt{m}$)	(MPa)
5.00	3.72	408.12	0	59.65	513.65
6.75	3.77	382.75	75	69.41	
11.40	3.80	342.00	120	102.28	

affected region.

The crack growth, stress decay, and K parameters are affected by fibre orientation, as shown in Fig. 4. The curve shows the remote stress (Fig. 4a) and the inherent crack length rate (Fig. 4b) as a function of the number of cycles. The standard deviation was captured based on the variability of unnotched laminate strength values using FFM model. The laminate [±45/0/90] exhibits an abrupt stress decay compared with cross-ply laminate, indicating a higher sensitivity in residual strength as a function of damage growth for quasi-
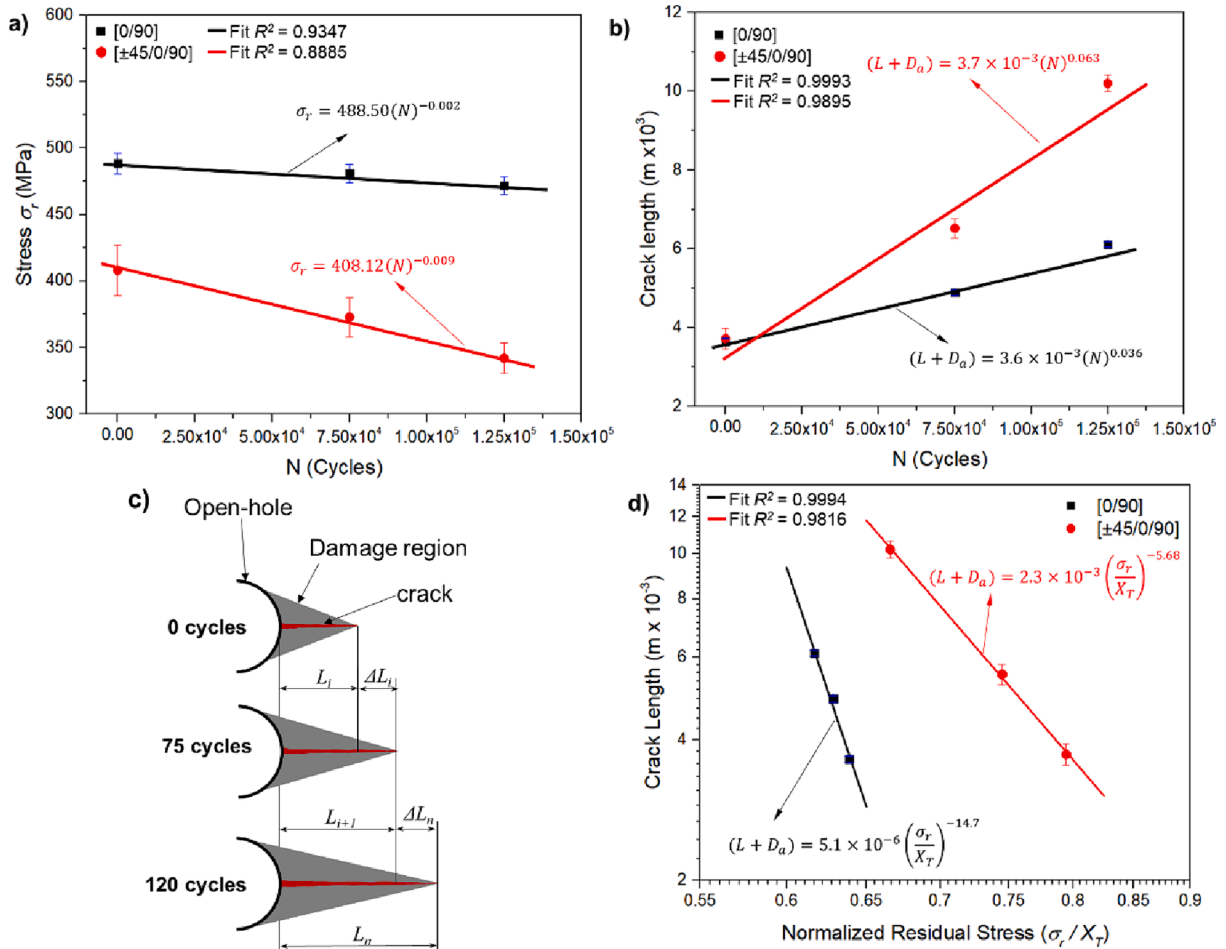

Fig. 4. a) Ultimate stress *versus* cycles (*N*), b) crack length (*L*) *versus* cycles (*N*), c) scheme of the crack length development as a function of cycles, and d) crack length *versus* normalised residual stress.

isotropic plates. The decay behaviour was modelled following the fit of $\sigma_r = 408.12(N)^{-0.009}$ and $\sigma_r = 488.50(N)^{-0.002}$ for $[\pm45/0/90]$ and $[0/90]$, respectively. In other words, the C_1 values are 408.12 for the $[\pm45/0/90]$ configuration and 488.50 for the $[0/90]$ configuration, meanwhile n_1 is -0.009 for quasi-isotropic specimen and -0.002 for cross-ply composite. The difference in stress decay and corresponding constants is related to the higher stiffness of the cross-ply configuration, which presents a higher concentration of fibres aligned in the direction of load application, keeping the stress close to the initial value even after damage initiation.

The results obtained using both equations are plotted in Fig. 4a and show a negative exponent reflecting residual stress decay due to cyclic loading induced by damage growth. The cross-ply laminate shows a low stress decay rate (in terms of number of cycles) associated with high crack growth. This behaviour is attributed to the ability of composites to maintain their structural behaviour even in the presence of cumulative damage [34,35]. On the other hand, the laminate $[\pm45/0/90]$ exhibits a high residual stress decay rate for low crack growth, directly related to the delamination in the stacking sequence and the formation of a larger damaged area caused during cyclic loading. The relation of the SIF lifecycle was determined experimentally by fitting the values of K_I *versus* number of cycles, and the reduction provides the following equation: cross-ply $K_{IC} = 71.2(N)^{0.015}$ and for quasi-isotropic plates $K_{IC} = 59.19(N)^{0.031}$, where the values of C_2 and n_2 are the fitting constants.

Fig. 4b shows the relation between crack size and the number of cycles. In particular, the $[\pm45/0/90]$ laminate exhibits a low exponential growth factor of crack length as a function of the number of cycles $(L + D_a) = 3.7 \bullet 10^{-3}(N)^{0.063}$, when compared to the $[0/90]$ laminate, where $(L + D_a) = 3.6 \bullet 10^{-3}(N)^{0.036}$. In addition, the multiaxial laminate also exhibits brittle behaviour, but the higher
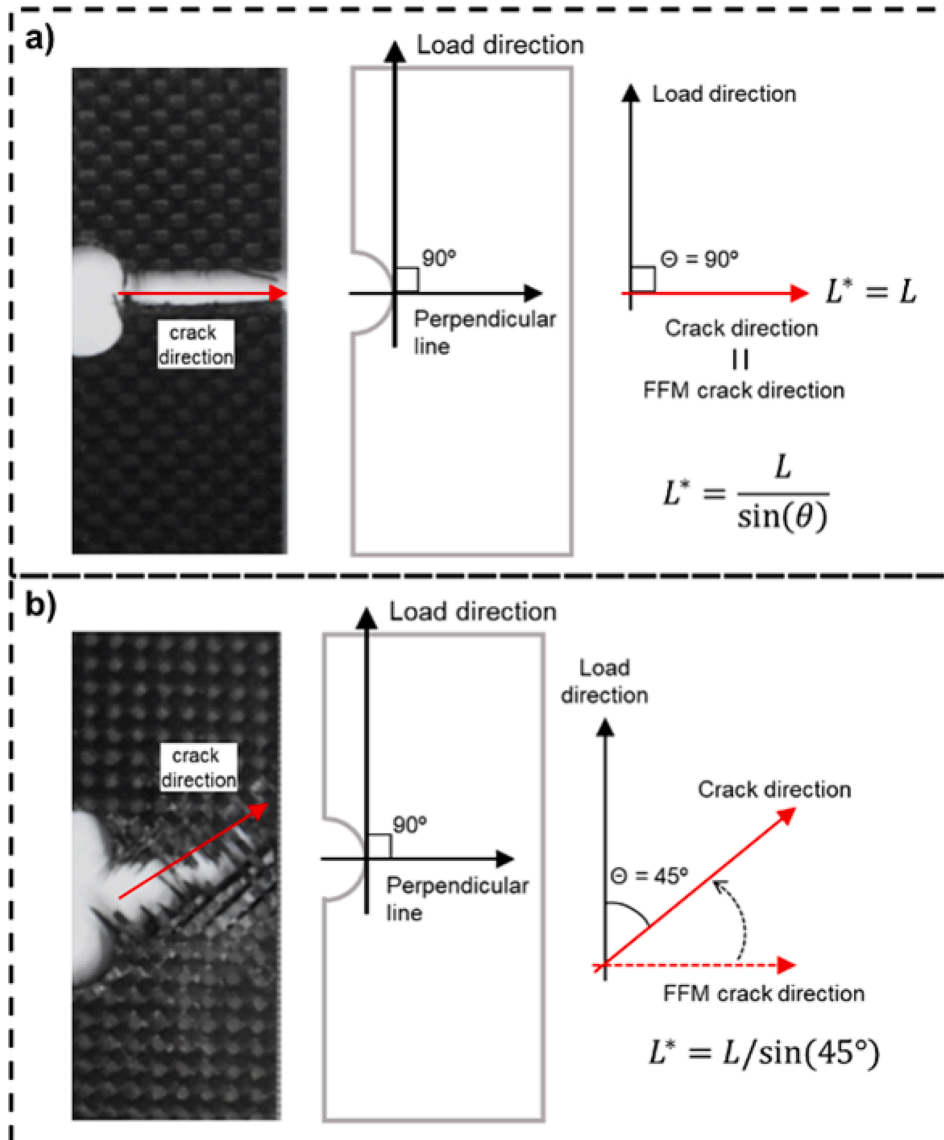

Fig. 5. Crack orientation: a) $[0/90]$ and b) $[\pm45/0/90]$.

stress suggests that the quasi-isotropic laminate is more sensitive to the presence of damage, particularly in the form of interlaminar damage [36,37]. Fig. 4c shows the scheme of the crack length development as a function of the cycles, where L_i values are extracted from the static tests and the ΔL_i is captured from the difference between the previous and current cycle number.

The delamination failure mode plays an important role in fatigue fracture analysis [38]. The interface regions between plies are more susceptible to delamination mechanisms. This is because their mechanical/chemical interaction is weaker than fibre fracture. As a result, microcracking can occur in the matrix and between the plies during cyclic loading, resulting in stress reduction [39]. The multiaxial laminate has a higher shear modulus and is therefore more prone to delamination. This is because the interfacial shear is more rigid and cannot accommodate local deformation, leading to delamination failure [40,41]. Further analysis is carried out in the fractographic analysis section to assess the impact of the above effect.

Fig. 4d shows the normalised residual stress curve as a function of crack length. In this case, the residual stress is normalised based on the unnotched tensile stress of each laminate configuration (σ_r/X_T). Considering the experimental data, it is possible to associate an empirical model of the failure envelope. This model can predict the empirical behaviour of damage progression based on the unnotched material properties and the generated stress for both laminate architectures, which follows the same trend shown in Fig. 4a and 4b. The number of data selected is sufficient for the present analysis, considering the linear behaviour of the power law equation adopted in the double logarithmic curve (Fig. 4d), where additional points would not significantly affect the behaviour of the curve (constants C_i and n_i).

4.3. Crack propagation orientation

The analysis of laminates with cross-ply fibre orientation revealed findings consistent with literature research [21], indicating that the fracture region is perpendicular to the direction of loading, i.e. translaminar failure behaviour. However, laminates with multiaxial fibre orientation shows a distinct behaviour, where continuous interlaminar shear and splitting along the fibre orientation formed under fatigue loading changes the crack direction. It is also important to be aware of the limitations of simplified stress analysis. It cannot accurately represent the effect of local corner geometry (particularly the angle of opening) [23]. The angle produced by the effect of fibre orientation is a determining factor to provide the crack direction and proper crack length, as illustrated in Fig. 5. The fibres oriented at $\pm$ 45 significantly influenced the crack direction, forcing it to follow the same angle, i.e., 45°.

Considering the fracture patterns resulting from laminate lay-up, it is possible to consider a revised crack length from a geometric point of view: $L^* = L/\sin(\theta)$, where θ is the angle between the observed crack and the load directions, L is the FFM crack length, and L^* is the revised crack length considering the current crack orientation. Therefore, it is possible to obtain a correction to the previously proposed Eq. (1) by considering the crack orientation shown in Eq. (12). If the crack is perpendicular to the loading direction, the angle $\theta = 90°$, and Eq. (12) becomes equal to the equation proposed in ref. [21]. In other words, for cracks perpendicular to the loading direction, the revised crack length is equal to the FFM crack size ($L^*= L$). However, the revised crack length provides the advantage of considering new directions of the propagation front.

$$\int_{R}^{R+L^*} \sigma_{yy}(x,0)dx = X_T \bullet L^*; L^* = L/sin(\theta) \tag{12}$$

By correcting for the crack direction, the values found for cross-ply laminates remain the same, considering that the direction of propagation is perpendicular to the direction of loading. For the quasi-isotropic laminate, the correction is generated and consequently all crack size (L) and effective K_{IC} values are modified according to Table 3. As a result of the correction, new relationships between crack propagation, SIF, stress and cycles are established: $(L+D_a) = 4.3 \bullet 10^{-3}(N)^{0.056}$, $K_{IC} = 55.72(N)^{0.036}$, $(L+D_a) = 1.3 \bullet 10^{-3}(\sigma_r/X_T)^{-5.14}$. The presented model can be applied to different types of delamination, reinforcement and architecture. It corrects for new mechanical properties using F_1 and F_2 factors and predicts crack propagation length behaviour based on experimental ultimate stress and SIF (K_{IC}) of the new configuration. The proposed FFM model adds a crack direction correction factor consistent with the fibre orientation used in the lay-up. It is a versatile method to evaluate the translaminar crack propagation for structural composite.

4.4. Paris model approach

The fracture behaviour in open-hole laminates is challenging because the damage occurs suddenly, making it difficult to accurately monitor its progress [42,43]. However, the FFM model in a cyclic approach makes it possible to create a predictive model for crack growth in laminates with open-hole. This approach enables the control of damage growth and life estimation. The model establishes a relationship between the crack propagation rate and the increase in the strain energy ratio (ΔK), allowing for predicting the remaining

Table 3
Experimental results for quasi-isotropic configuration.

D_a	L	σ_r	Cycles N	K_{IC}	X_T
(mm)	(mm)	(MPa)	($\times 10^3$)	(MPa$\bullet \sqrt{m}$)	(MPa)
5.00	4.37	408.12	0	56.20	513.65
6.75	4.43	382.75	75	67.37	
11.40	4.47	342.00	120	103.83	

service life of a component or structure subject to cyclic loading. This method considers the gradual and increasing propagation of L generated by damage growth over the cycle. The interpolation of the curve in Fig. 3a provides the crack propagation rate (dL/dN). The Paris law ($da/dN = A \bullet \Delta K^{\beta}$) [16,44] was used to formulate the crack propagation rate as a function of the similitude parameter ΔK, considering the crack growth rate (a), which is directly related to the crack length ($L + D_a$).

The adjustment in crack direction gives a relation between crack length and stress/energy. The damage propagation rate $d(L^*+Da)/dN$ versus the stress intensity factor rate (ΔK) is shown in Fig. 6. This analysis created a more realistic empirical power law model for each laminate configuration, which estimates the damage progression behaviour based on the properties of the unnotched material and the stress generated by the material. Considering the crack direction, the increase in the size of the damage is inversely proportional to the residual stress decay. This fit preserves the behaviour observed in the [0/90] laminate, establishing an appropriate relation between crack size and the residual stress decay in the [±45/0/90] laminate. In addition, the number of data selected is sufficient for the present analysis, considering the linear section II of Paris curve adopted in the double logarithmic curve (Fig. 6), where additional points should not affect the behaviour of the curve, i.e., the constants A and β.

Considering the revised crack length direction, the coefficients of the Paris curve also changed, resulting in a more accurate comparative analysis of laminate architecture considering the damage propagation in an open-hole configuration. For the cross-ply laminate, shown the Paris coefficients were A = 10^{-17} (m/cycle) and β = 5.32. On the other hand, for the [±45/0/90] laminate, the constants are A = $9 \cdot 10^{-14}$ (m/cycle) and β = 3.27, following the correction of damage direction. The quasi-isotropic laminate presents better control of fatigue damage growth, making it more resistant to damage propagation than the cross-ply configuration. The quasi-isotropic laminate requires more energy for crack propagation due to the angular relationship between loading and crack direction, resulting in mixed-mode fracture. This is in contrast to the cross-ply laminate, which exhibits pure mode I translaminar fracture.

4.5. Fractographic analysis

Based on the predictions and trends presented earlier, a correlation between the failure mechanisms and the experimental analysis is detailed in this section. Fig. 7 illustrates the ½ section of the open-hole specimen, defining the mechanism observed during the initiation of matrix cracking (Stage I), subsequent crack growth via adhesive crack growth and splitting (Stage II), and eventual propagation of translaminar cracking (Stage III) after fibre isolation and energy threshold are reached [45]. Fig. 7 highlights the variability in the formation and growth of splitting under cyclic loading as a function of fibre orientation.

During the initial cycles, splitting growth is concentrated longitudinally, with isolated fibres increasing the susceptibility to fracture (Fig. 7a - [0/90]). On the other hand, the [±45/0/90] laminate exhibits splitting propagation in multiple directions, reflecting the fibre orientation effect. However, the distributions of stage I and II fracture mechanisms are larger and in X-pattern shape compared to the cross-ply laminate. This results in a delayed propagation of translaminar cracks. The literature corroborates these findings, as Llobet et al. [46] reported the absence of catastrophic failure even after high cycle numbers. They suggested that the development of fatigue damage and splitting reduces the stress concentration and mitigates fibre failure. This trend is also evident in Fig. 8, which displays the fractured laminates under static and cyclic loading.

Fig. 8a exhibits the cross-ply laminate, with translaminar damage propagation perpendicular to the crack direction, as expected from the FFM model equations. However, the [±45/0/90] laminate (Fig. 8b) showed a shift in the direction of fracture based on fibre orientation. This trend is attributed to splitting in the corresponding directions (X-pattern), generating a region more susceptible to crack growth. At 120 k cycles, the amount of splitting prevented the translaminar fracture (fibre fracture – Fig. 8b) due to internal damage mechanisms such as fibre detachment and layer delamination. This behaviour indicates a cycle level dependence to create sufficient delamination and splitting mechanisms to prevent the translaminar fracture.
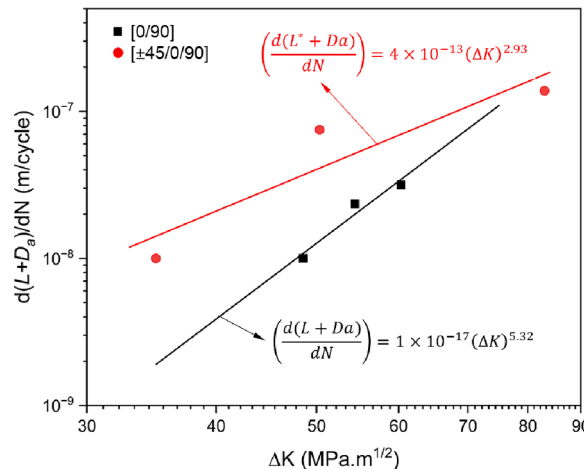

The figure shows a double logarithmic plot of $d(L+D_a)/dN$ (m/cycle) versus ΔK (MPa·m$^{1/2}$). Legend: ■ [0/90], ● [±45/0/90]. Red curve equation: $\left(\dfrac{d(L^* + Da)}{dN}\right) = 4 \times 10^{-13}(\Delta K)^{2.93}$. Black curve equation: $\left(\dfrac{d(L + Da)}{dN}\right) = 1 \times 10^{-17}(\Delta K)^{5.32}$.

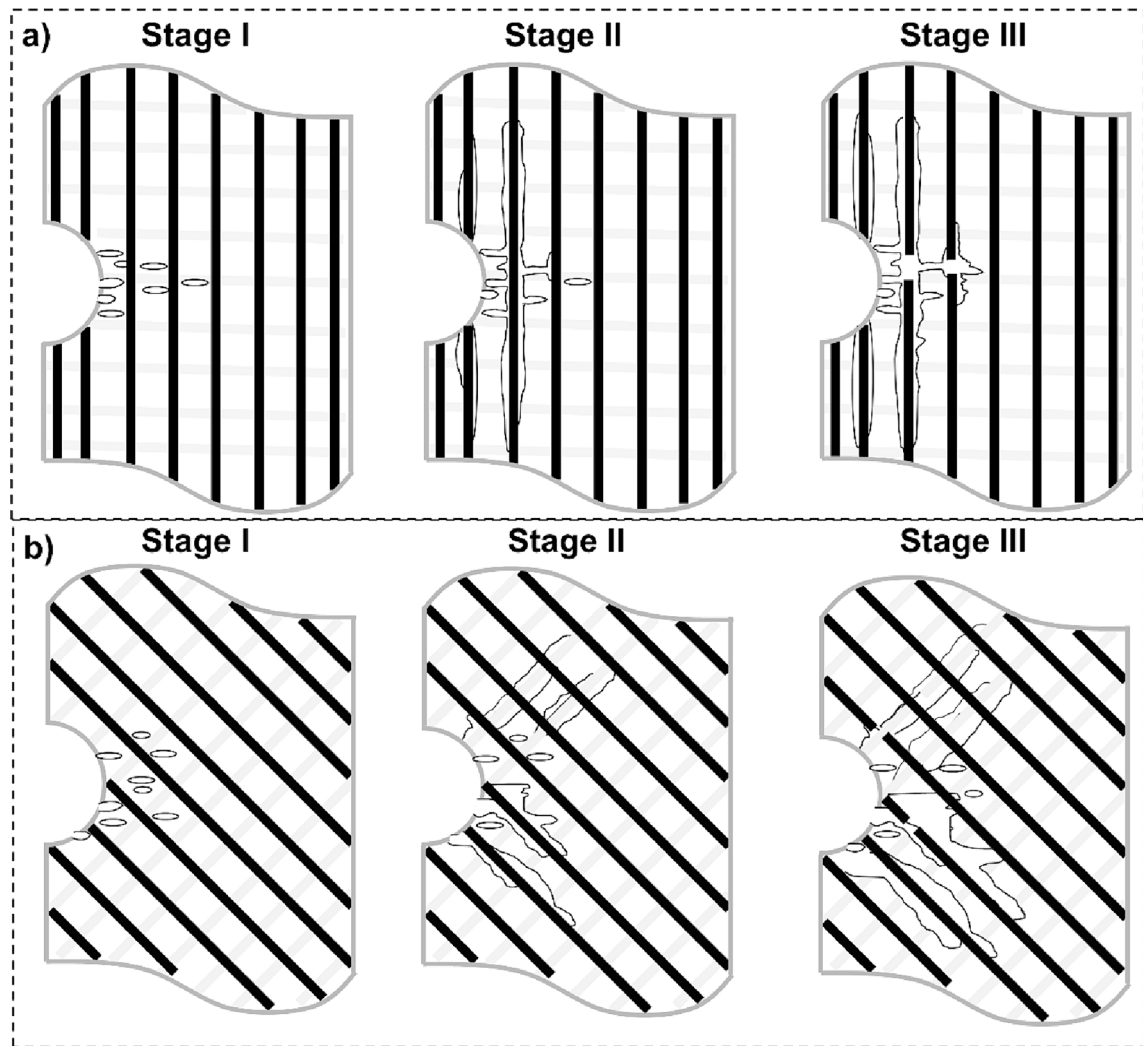**Fig. 6.** Crack propagation rate *versus* stress intensity factor.

Fig. 7. Illustration of the development of damage under fatigue loading: a) [0/90] and b) [±45/0/90].

Fig. 9 illustrates the delamination behaviour, as shown by the fracture surface in the thickness cross-section area. Fig. 9a and 9b show the fracture section of the [0/90] laminate, while Fig. 9c and 9d exhibit the fracture surfaces of the [±45/0/90] laminate. Fig. 9a and 9b present a dominance of translaminar fracture. Despite the cyclic loading, the laminate configuration maintains the stress concentration, and the damage propagates perpendicular to the fibres. This phenomenon is typical of laminates subjected to static loading, where the open-hole strength is governed by the translaminar cohesive law with fibre fracture [47]. In contrast, the [±45/0/90] laminate demonstrates a predominance of delamination damage caused by the shear mismatch between multi-oriented layers and cyclic loading. In particular, the second laminate shows a greater dependence on the cycle level, producing a fluctuation between intra and interlaminar failure modes. Fatigue damage in open-hole specimens is influenced by the progressive growth of splitting and delamination as a function of fibre orientation [48,49].

García-Carpintero et al. [50] have reported that the material architecture influences the damage mechanisms and fracture toughness, which are also influenced by the direction of crack propagation. The fracture path in translaminar fracture is non-linear and follows the zig-zag pattern of the yarn architecture in the direction of the fibre. Woven fabrics are another critical factor, mainly because of the weft/warp intersection point, which can prevent further crack propagation. The crack will naturally move in the direction with the lowest energy, typically found in adhesive fracture [51,52]. However, propagation could change direction when the crack front assembles the perpendicular fibres. Thus, additional energy is required each time the crack direction changes [50,53]. This behaviour is evident in the laminate [±45/0/90], which exhibits splitting formation in several directions, as the multi-directional of the fibres enhances the likelihood of the crack stopping at the fibre interface and migrating to another splitting region, occasionally propagating between layers.

The laminate fracture propagation paths for the cross-ply laminate (Fig. 10a and 10b) and [±45/0/90] (Fig. 10c and 10d) showed different fracture paths for each fibre orientation. The broom pattern observed in the cross-ply laminates is derived from the degree of
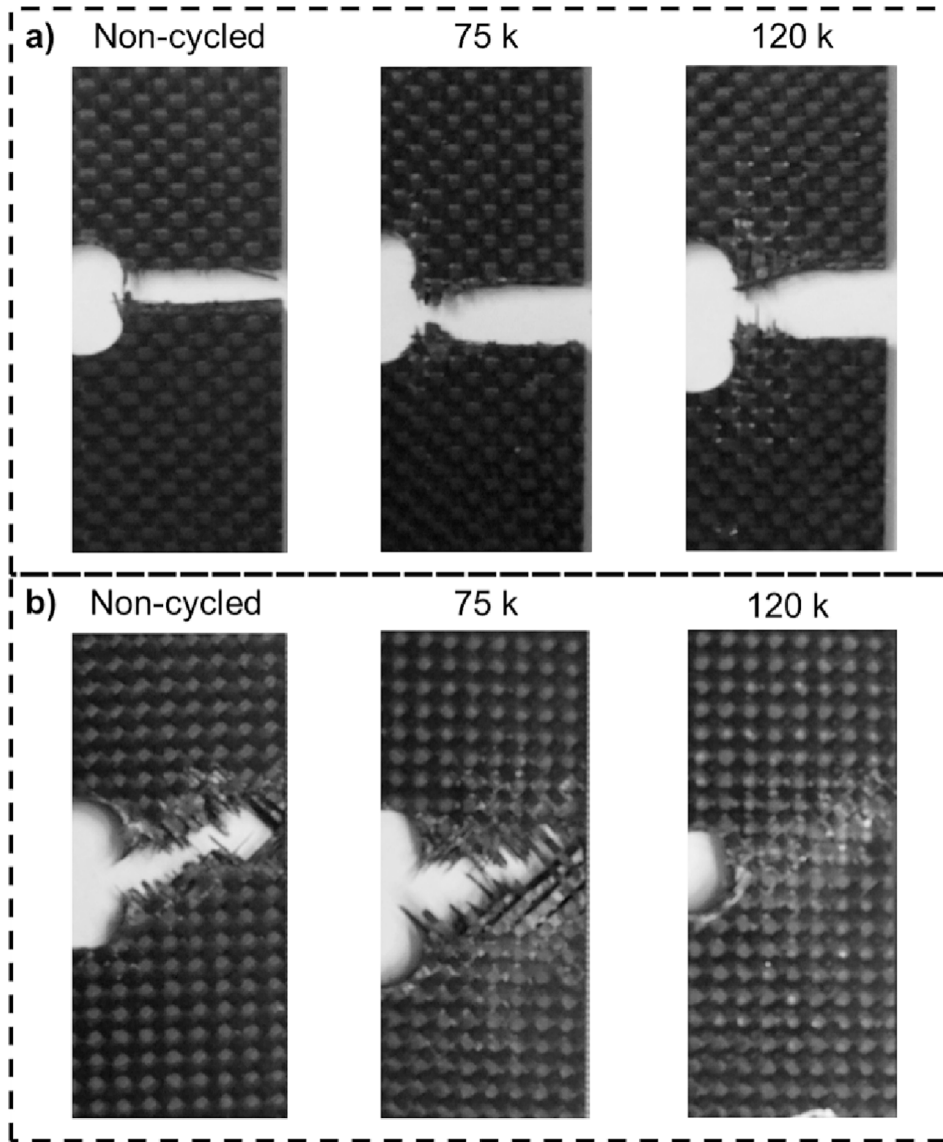
Fig. 8. Damaged composite after static and fatigue loading: a) [0/90] and b) [±45/0/90].

ply splitting, which occurs prior to fibre fracture. This pattern exhibits fractures at the horizontal interface of the plies and longitudinal splitting with radial marks due to debonding patterns on individual filaments, resulting in fibre breakage at several heights [54,55]. In contrast, the [±45/0/90] laminate propagates the cracks in a sawtooth pattern that coincides with the orientation of the fibres. The sawtooth pattern consists of notches corresponding to longitudinal fractures of the bias plies, presenting an angular variation of 45°. This angle can be deduced from the parallel direction of the fractures in each bias ply. The tortuosity of the [±45/0/90] laminate propagation path is directly related to the prevention of damage propagation, resulting in the interaction of failure mechanism modes [56].

5. Conclusions

The open-hole tensile fatigue test was experimentally investigated for two lay-up configurations. From the experimental study, the following conclusions can be drawn:

- C-scan analysis and crack propagation direction revision proved to be key approaches in determining the most realistic crack growth behaviour for multidirectional lay-up;
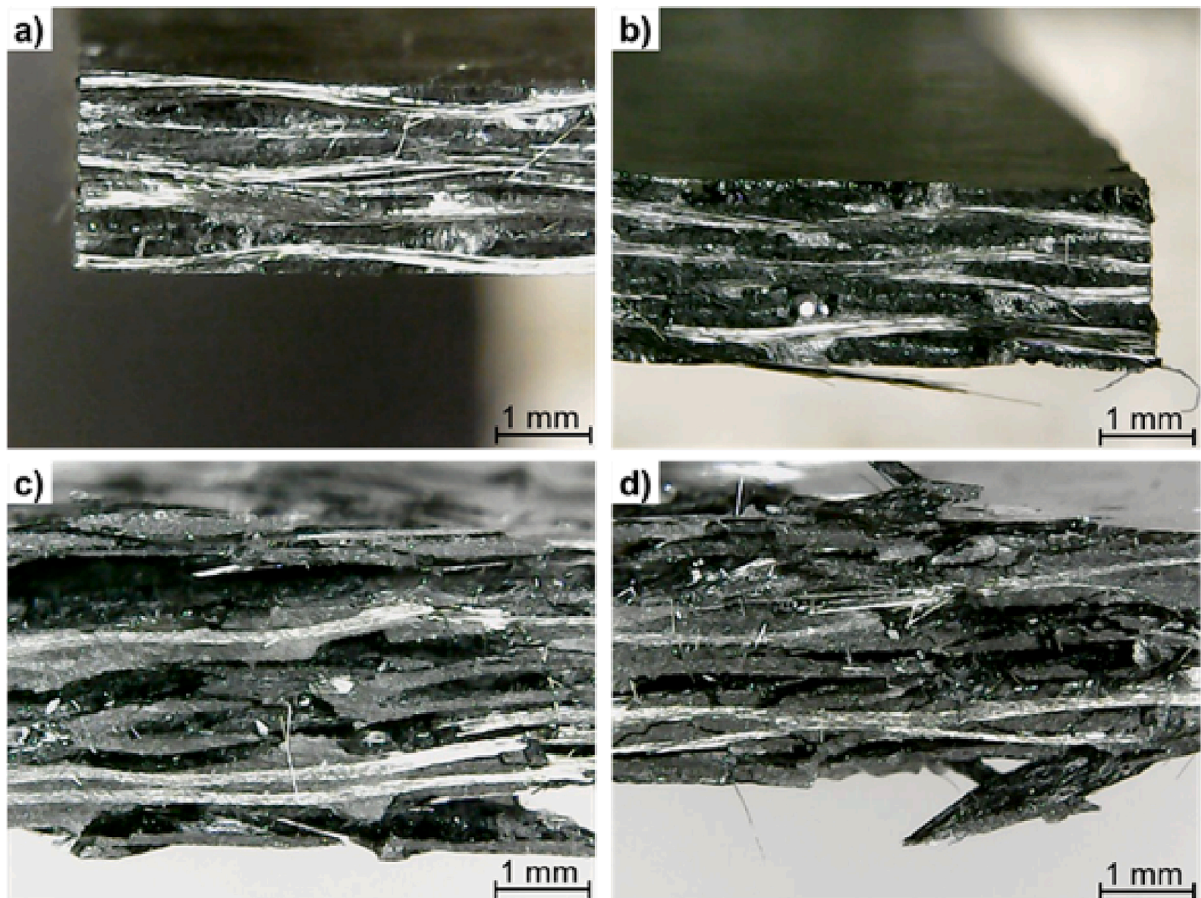
Fig. 9. Fractured surface (thickness section): a-b) [0/90] and c-d) [±45/0/90].

- This work contribution is also related to the application of the Paris model (based on dL/dN and SIF for each cycle) to generate the damage propagation rate curve in relation to the strain energy release ratio and thus generate a translaminar damage propagation prediction model.
- The study focused on damage mechanisms in [±45/0/90] composites during cyclic loading, emphasising splitting as the main damage pattern. In addition, quasi-isotropic laminates showed superior control of crack propagation rates due to their ability to reduce residual stress and exhibit mixed-mode fracture behaviour resulting from the angular relationship between load and crack orientation.
- The cross-ply laminate exhibited a broom pattern attributed to the transverse splitting prior to fibre fracture. Conversely, the [±45/0/90] laminate showed a sawtooth pattern in the propagation path, directly influenced by the fibre orientation.

CRediT authorship contribution statement

Francisco Maciel Monticeli: Writing – original draft, Visualization, Validation, Methodology, Investigation, Formal analysis, Data curation, Conceptualization. **Felipe Ruivo Fuga:** Writing – review & editing, Validation, Methodology, Formal analysis. **Mariano Andrés Arbelo:** Writing – review & editing, Methodology, Conceptualization. **Maurício Vicente Donadon:** Writing – review & editing, Supervision, Resources, Project administration, Funding acquisition, Conceptualization.

Declaration of competing interest

Data availability

Data will be made available on request.
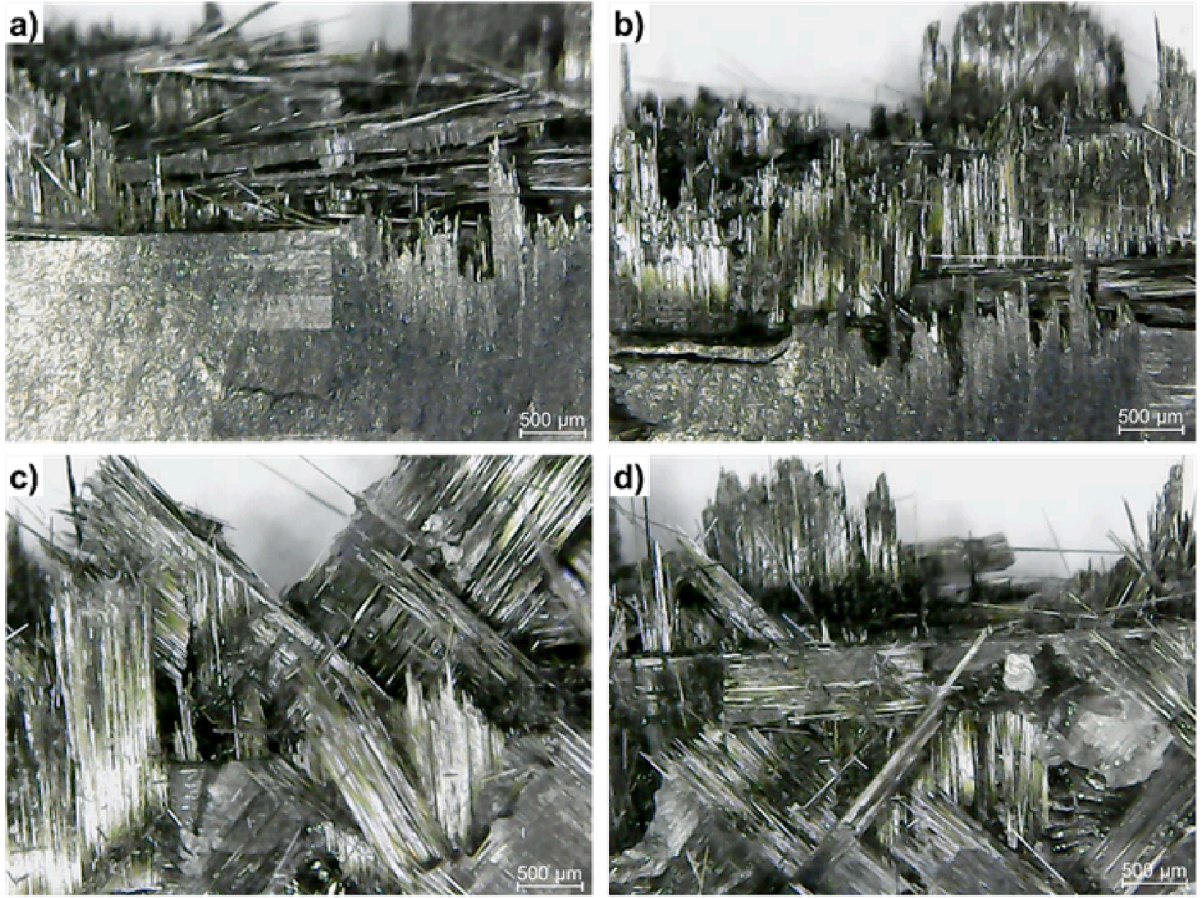
Fig. 10. Fractured surface (width section): a-b) [0/90] and c-d) [±45/0/90].

Appendix A

Following the classical laminate theory (CLT), Eq. (A1) shows the stiffness matrix (*A*), bending-extension coupling matrix (*B*), and bending stiffness matrix (*D*) associated with the in-plane force vector $N = [N_x, N_y, N_{xy}]^T$ and bending moment vector $M = [M_x, M_y, M_{xy}]^T$, both related to the in-plane strain vector $\varepsilon = [\varepsilon_x, \varepsilon_y, \varepsilon_{xy}]^T$ and curvature vector $\kappa = [\kappa_x, \kappa_y, \kappa_{xy}]^T$, shown in Equation:

$$\begin{Bmatrix} N_x \\ N_y \\ N_{xy} \end{Bmatrix} = \begin{Bmatrix} A_{11} & A_{12} & A_{16} \\ A_{21} & A_{22} & A_{26} \\ A_{16} & A_{26} & A_{66} \end{Bmatrix} \begin{Bmatrix} \varepsilon_x \\ \varepsilon_y \\ \gamma_{xy} \end{Bmatrix} + \begin{Bmatrix} B_{11} & B_{12} & B_{16} \\ B_{21} & B_{22} & B_{26} \\ B_{16} & B_{26} & B_{66} \end{Bmatrix} \begin{Bmatrix} \kappa_x \\ \kappa_y \\ \kappa_{xy} \end{Bmatrix}$$

$$\begin{Bmatrix} M_x \\ M_y \\ M_{xy} \end{Bmatrix} = \begin{Bmatrix} B_{11} & B_{12} & B_{16} \\ B_{21} & B_{22} & B_{26} \\ B_{16} & B_{26} & B_{66} \end{Bmatrix} \begin{Bmatrix} \varepsilon_x \\ \varepsilon_y \\ \gamma_{xy} \end{Bmatrix} + \begin{Bmatrix} D_{11} & D_{12} & D_{16} \\ D_{21} & D_{22} & D_{26} \\ D_{16} & D_{26} & D_{66} \end{Bmatrix} \begin{Bmatrix} \kappa_x \\ \kappa_y \\ \kappa_{xy} \end{Bmatrix} \tag{A1}$$

The relations between these properties and the elements of the matrix A are given by:

$$A_{11} = \frac{E_1}{1 - v_{12}v_{21}} \tag{A2}$$

$$A_{12} = \frac{v_{12}E_2}{1 - v_{12}v_{21}} \tag{A3}$$

$$A_{22} = \frac{E_1}{1 - v_{12}v_{21}} \tag{A4}$$

$$A_{66} = G_{12} \tag{A5}$$

After calculating the elements of matrix A for each individual laminate, we can determine the equivalent laminate properties. The equations to calculate these equivalent properties in terms of the elements of matrix A are as follows:

$$E_x = \frac{1}{h}(A_{11}t_1 + A_{12}t_2) \tag{A6}$$

$$E_y = \frac{1}{h}(A_{12}t_1 + A_{22}t_2) \tag{A7}$$

$$G_{12} = \frac{1}{h}A_{66} \tag{A8}$$

$$v_{12} = \frac{-A_{12}}{A_{11}} \tag{A9}$$

where, h is the total thickness of the laminate, t_1 and t_2 are the thicknesses of layers 1 and 2 respectively.

Appendix B

Fig. A1 shows the procedure to measure the equivalent diameter (D_a) from C-scan images using ImageJ software. The First image shows the C-scan image, and provide the scale based on the width section (50 mm). The second one was applied threshold colour to filter the blue areas (regions in which there is delamination), which was in the range of 129–185. Then the image was converted to 8-bits RGB coloured, so we keep the colour but provide a simpler weave to work with threshold. The following step was applying the second threshold to highlight the red region and remove the rest. Based on the black dots, it was possible to measure the equivalent area, which was associated with the area of the circle, as shown in the las image (equivalent diameter of delamination fracture).
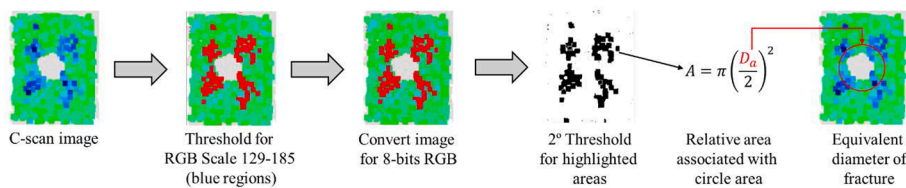

Fig. A1. Sequence of equivalent diameter measurement from C-scan images.

References

[1] G. Sun, X. Xia, X. Liu, Q. Luo, Q. Li, On quasi-static behaviors of different joint methods for connecting carbon fiber reinforce plastic (CFRP) laminate and aluminum alloy, Thin-Walled. Struct. 164 (2021) 107657, https://doi.org/10.1016/J.TWS.2021.107657.
[2] C. Soutis, Carbon fiber reinforced plastics in aircraft construction, Mater. Sci. Eng. A 412 (2005) 171–176, https://doi.org/10.1016/J.MSEA.2005.08.064.
[3] J.L. Kasan, K.A. Harries, R. Miller, R.J. Brinkman, Limits of application of externally bonded CFRP repairs for impact-damaged prestressed concrete girders, J. Compos. Constr. 18 (2012), https://doi.org/10.1061/(ASCE)CC.1943-5614.0000347. A4013013.
[4] S. Tian, C. Li, W. Dai, D. Jia, H. Zhang, M. Xu, et al., Effect of the countersunk hole depth on tensile-tensile fatigue behavior of riveted specimens of AA2024-T3 alloy, Eng. Fail. Anal 115 (2020) 104639, https://doi.org/10.1016/J.ENGFAILANAL.2020.104639.
[5] F. Darwish, G. Tashtoush, G. Gharaibeh, Stress concentration analysis for countersunk rivet holes in orthotropic plates, Eur. J. Mech. –. A/solids 37 (2013) 69–78, https://doi.org/10.1016/J.EUROMECHSOL.2012.04.006.
[6] M. Li, S. Li, X. Yang, The influence of machining processes on strain distribution and progressive failure characteristics when producing holes in CFRP, Compos. Struct 238 (2020) 111994, https://doi.org/10.1016/J.COMPSTRUCT.2020.111994.
[7] V. Mára, L. Michalcová, M. Kadlec, J. Krčil, P. Špatenka, The effect of long-time moisture exposure and low temperatures on mechanical behavior of open-hole Cfrp laminate, Polym. Compos 42 (2021) 3603–3618, https://doi.org/10.1002/PC.26082.
[8] M. Rezasefat, M. Giglio, A. Manes, Numerical investigation of the effect of open holes on the impact response of CFRP laminates, Appl. Compos. Mater. 29 (2022) 1555–1578, https://doi.org/10.1007/S10443-022-10031-6/FIGURES/18.
[9] S.T. Pinho, P. Robinson, L. Iannucci, Fracture toughness of the tensile and compressive fibre failure modes in laminated composites, Compos. Sci. Technol 66 (2006) 2069–2079, https://doi.org/10.1016/J.COMPSCITECH.2005.12.023.
[10] P. Maimí, A. Ortega, E.V. González, J. Costa, Should the translaminar fracture toughness of laminated composites be represented by the R or the J curve? a comparison of their consistency and predictive capability, Compos. Part. A. Appl. Sci. Manuf 156 (2022) 106867, https://doi.org/10.1016/J.COMPOSITESA.2022.106867.
[11] F.M. Monticeli, F.R. Fuga, M.V. Donadon, A systematic review on translaminar fracture damage propagation in fiber-reinforced polymer composites, Thin-Walled. Struct. 187 (2023) 110742, https://doi.org/10.1016/J.TWS.2023.110742.
[12] F.P. van der Meer, Mesolevel modeling of failure in composite laminates: constitutive, kinematic and algorithmic aspects. Arch. Comput. Methods Eng. 2012 19: 3 2012;19:381–425. 10.1007/S11831-012-9076-Y.
[13] S.W. Tsai, E.M. Wu, A general theory of strength for anisotropic materials, J. Compos. Mater. 5 (1971) 58–80, https://doi.org/10.1177/002199837100500106.

[14] A.A. Griffith, The Phenomena of Rupture and Flow in Solids. vol. 221, 1921.

[15] G.R. Irwin, Onset of fast crack propagation in high strength steel and aluminum alloys, Naval Res. Laborat. –.Tech. Library Res. Rep. Sect. (1956) 1–23.

[16] P.C. Paris, The Fracture Mechanics Approach to Fatigue, Syracuse University Press, Raquette Lake, NY, 1964, p. 26.

[17] K.Y. Chang, S. Llu, F.K. Chang, Damage tolerance of laminated composites containing an open hole and subjected to tensile loadings, J. Compos. Mater. 25 (1991) 274–301, https://doi.org/10.1177/002199839102500303.

[18] J.M. Whitney, R.J. Nuismer, Stress fracture criteria for laminated composites containing stress concentrations, J. Compos. Mater. 8 (1974) 253–265, https://doi.org/10.1177/002199837400800303.

[19] D. Leguillon, Strength or toughness? a criterion for crack onset at a notch, Eur. J. Mech. A. Solids 21 (2002) 61–72, https://doi.org/10.1016/S0997-7538(01)01184-6.

[20] P.P. Camanho, P. Maimí, C.G. Dávila, Prediction of size effects in notched laminates using continuum damage mechanics, Compos. Sci. Technol 67 (2007) 2715–2727, https://doi.org/10.1016/J.COMPSCITECH.2007.02.005.

[21] P.P. Camanho, G.H. Erçin, G. Catalanotti, S. Mahdi, P. Linde, A finite fracture mechanics model for the prediction of the open-hole strength of composite laminates, Compos. Part. A. Appl. Sci. Manuf 43 (2012) 1219–1225, https://doi.org/10.1016/J.COMPOSITESA.2012.03.004.

[22] B. Vieille, J.D. Pujols Gonzalez, C. Bouvet, Prediction of the ultimate strength of quasi-isotropic TP-based laminates structures from tensile and compressive fracture toughness at high temperature, Compos. B Eng. 164 (2019) 437–446, https://doi.org/10.1016/J.COMPOSITESB.2019.01.056.

[23] K. Tserpes, A. Barroso-Caro, P.A. Carraro, V.C. Beber, I. Floros, W. Gamon, et al., A review on failure theories and simulation models for adhesive joints, J. Adhes. 98 (2022) 1855–1915, https://doi.org/10.1080/00218464.2021.1941903.

[24] P. Cornetti, N. Pugno, A. Carpinteri, D. Taylor, Finite fracture mechanics: a coupled stress and energy failure criterion, Eng. Fract. Mech 73 (2006) 2021–2033, https://doi.org/10.1016/J.ENGFRACMECH.2006.03.010.

[25] B.G. Green, M.R. Wisnom, S.R. Hallett, An experimental investigation into the tensile strength scaling of notched composites, Compos. Part. A. Appl. Sci. Manuf 38 (2007) 867–878, https://doi.org/10.1016/J.COMPOSITESA.2006.07.008.

[26] A.M. Mirzaei, P. Cornetti, A. Sapora, A novel finite fracture mechanics approach to assess the lifetime of notched components, Int. J. Fatigue 173 (2023) 107659, https://doi.org/10.1016/J.IJFATIGUE.2023.107659.

[27] R.R.R. Souza, S.L. Nascimento Junior, N.N.A. Silveira, M.A. Arbelo, M.V. Donadon, Translaminar fracture toughness and fatigue crack growth characterization of carbon-epoxy plain weave laminates, Polym. Compos 40 (2019) 3791–3804, https://doi.org/10.1002/pc.25247.

[28] J. Galos, Thin-ply composite laminates: a review, Compos. Struct 236 (2020) 111920, https://doi.org/10.1016/J.COMPSTRUCT.2020.111920.

[29] G. Lee, M. Sung, J.H. Youk, J. Lee, W.R. Yu, Improved tensile strength of carbon nanotube-grafted carbon fiber reinforced composites, Compos. Struct 220 (2019) 580–591, https://doi.org/10.1016/J.COMPSTRUCT.2019.04.037.

[30] V. Achard, C. Bouvet, B. Castanié, C. Chirol, Discrete ply modelling of open hole tensile tests, Compos. Struct 113 (2014) 369–381, https://doi.org/10.1016/J.COMPSTRUCT.2014.03.031.

[31] R. Gutkin, S.T. Pinho, P. Robinson, P.T. Curtis, A finite fracture mechanics formulation to predict fibre kinking and splitting in CFRP under combined longitudinal compression and in-plane shear, Mech. Mater. 43 (2011) 730–739, https://doi.org/10.1016/J.MECHMAT.2011.08.002.

[32] P. Colombi, G. Fava, L. Sonzogni, Fatigue crack growth in CFRP-strengthened steel plates, Compos. B. Eng 72 (2015) 87–96, https://doi.org/10.1016/J.COMPOSITESB.2014.11.036.

[33] J.S. Fenner, I.M. Daniel, Hybrid nanoreinforced carbon/epoxy composites for enhanced damage tolerance and fatigue life, Compos. Part. A. Appl. Sci. Manuf 65 (2014) 47–56, https://doi.org/10.1016/J.COMPOSITESA.2014.05.023.

[34] A. Hosoi, H. Kawada, H. Yoshino, Fatigue characteristics of quasi-isotropic CFRP laminates subjected to variable amplitude cyclic two-stage loading, Int. J. Fatigue 28 (2006) 1284–1289, https://doi.org/10.1016/J.IJFATIGUE.2006.02.039.

[35] J. Noda, M. Nakada, Y. Miyano, Fatigue Life Prediction under Variable Cyclic Loading Based on Statistical Linear Cumulative Damage Rule for CFRP Laminates n.d. 10.1177/0731684407075577.

[36] S.R. Choi, J.A. Salem, Slow crack growth of indent cracks in glass with and without applied stress, Mater. Sci. Eng. A 149 (1992) 259–264, https://doi.org/10.1016/0921-5093(92)90387-G.

[37] J. Salomonson, K. Zeng, D. Rowcliffe, Decay of residual stress at indentation cracks during slow crack growth in soda-lime glass, Acta. Mater 44 (1996) 543–546, https://doi.org/10.1016/1359-6454(95)00199-9.

[38] M.Y. Shiino, L.M. De Camargo, M.O.H. Cioffi, H.C.J. Voorwald, E.C. Ortiz, M.C. Rezende, Correlation of microcrack fracture size with fatigue cycling on non-crimp fabric/RTM6 composite in the uniaxial fatigue test, Compos. B Eng 43 (2012) 2244–2248, https://doi.org/10.1016/j.compositesb.2012.01.074.

[39] J.A. Pascoe, R.C. Alderliesten, R. Benedictus, Methods for the prediction of fatigue delamination growth in composites and adhesive bonds - a critical review, Eng. Fract. Mech 112–113 (2013) 72–96, https://doi.org/10.1016/j.engfracmech.2013.10.003.

[40] W. Hintze, D. Hartmann, Modeling of delamination during milling of unidirectional CFRP, Procedia CIRP 8 (2013) 444–449, https://doi.org/10.1016/J.PROCIR.2013.06.131.

[41] N. Takeda, S. Ogihara, Initiation and growth of delamination from the tips of transverse cracks in CFRP cross-ply laminates, Compos. Sci. Technol 52 (1994) 309–318, https://doi.org/10.1016/0266-3538(94)90166-X.

[42] C. Hochard, J. Payan, C. Bordreuil, A progressive first ply failure model for woven ply CFRP laminates under static and fatigue loads, Int. J. Fatigue 28 (2006) 1270–1276, https://doi.org/10.1016/J.IJFATIGUE.2006.02.024.

[43] R. Aoki, R. Higuchi, T. Yokozeki, Progressive damage and residual strength of open-hole thin-ply CFRP laminates under tensile fatigue loading, Compos. Struct 314 (2023) 116973, https://doi.org/10.1016/J.COMPSTRUCT.2023.116973.

[44] L. Yao, Y. Sun, L. Guo, M. Zhao, L. Jia, R.C. Alderliesten, et al., A modified Paris relation for fatigue delamination with fibre bridging in composite laminates, Compos. Struct 176 (2017) 556–564, https://doi.org/10.1016/j.compstruct.2017.05.070.

[45] Q. Han, L. Wang, J. Xu, Experimental research on fracture behaviors of damaged CFRP tendons: Fracture mode and failure analysis, Constr. Build. Mater 112 (2016) 1013–1024, https://doi.org/10.1016/j.conbuildmat.2016.03.036.

[46] J. Llobet, P. Maimí, Y. Essa, F. Martin de la Escalera, A continuum damage model for composite laminates: Part III - fatigue, Mech. Mater. 153 (2021) 103659, https://doi.org/10.1016/j.mechmat.2020.103659.

[47] A. Ortega, P. Maimí, E.V. González, D. Trias, Characterization of the translaminar fracture cohesive law, Compos. Part. A. Appl. Sci. Manuf. 91 (2016) 501–509, https://doi.org/10.1016/j.compositesa.2016.01.019.

[48] O.J. Nixon-Pearson, S.R. Hallett, An investigation into the damage development and residual strengths of open-hole specimens in fatigue, Compos. Part A Appl. Sci. Manuf. 69 (2015) 266–278, https://doi.org/10.1016/J.COMPOSITESA.2014.11.013.

[49] B. Aidi, M.K. Philen, S.W. Case, Progressive damage assessment of centrally notched composite specimens in fatigue, Compos. Part A Appl. Sci. Manuf 74 (2015) 47–59, https://doi.org/10.1016/J.COMPOSITESA.2015.03.022.

[50] A. García-Carpintero, B.N.G. van den Beuken, S. Haldar, M. Herráez, C. González, C.S. Lopes, Fracture behaviour of triaxial braided composites and its simulation using a multi-material shell modelling approach, Eng. Fract. Mech 188 (2018) 268–286, https://doi.org/10.1016/J.ENGFRACMECH.2017.08.034.

[51] F.M. Monticeli, H. Jacobus, C. Voorwald, The influence of carbon/glass/epoxy hybrid composite through mode I fatigue loading: physical-based characterization, Compos. Struct. (2021) 1.

[52] R. Khan, R. Alderliesten, R. Benedictus, Two-parameter model for delamination growth under mode i fatigue loading (Part a: Experimental study), Compos. Part A Appl. Sci. Manuf 65 (2014) 192–200, https://doi.org/10.1016/j.compositesa.2014.06.007.

[53] A. García-Carpintero, M. Herráez, J. Xu, S. Lopes, C. González, A multi material shell model for the mechanical analysis of triaxial braided composites, Appl. Compos. Mater. 24 (2017) 1425–1445, https://doi.org/10.1007/S10443-017-9593-9/FIGURES/12.

[54] M.S. Kumar, K. Raghavendra, M.A. Venkataswamy, H.V. Ramachandra, Fractographic analysis of tensile failures of aerospace grade composites, Mater. Res. 15 (2012) 990–997, https://doi.org/10.1590/S1516-14392012005000141.

[55] C.V. Opelt, G.M. Cândido, M.C. Rezende, Compressive failure of fiber reinforced polymer composites – a fractographic study of the compression failure modes, Mater. Today. Commun 15 (2018) 218–227, https://doi.org/10.1016/J.MTCOMM.2018.03.012.

[56] G. Bullegas, J. Benoliel, P.L. Fenelli, S.T. Pinho, S. Pimenta, Towards quasi isotropic laminates with engineered fracture behaviour for industrial applications, Compos. Sci. Technol 165 (2018) 290–306, https://doi.org/10.1016/j.compscitech.2018.07.004.